



A Novel Cu(II) Ion-Imprinted Alginate–Chitosan Complex Adsorbent for Selective Separation of Cu(II) from Aqueous Solution

Weiyang Zhang¹ · Mengying Yun¹ · Zhenlin Yu¹ · Dan Chen¹ · Xiao Li¹

Received: 16 November 2017 / Revised: 3 July 2018 / Accepted: 6 July 2018 / Published online: 3 August 2018
© Springer-Verlag GmbH Germany, part of Springer Nature 2018

Abstract

A novel Cu(II) ion-imprinted complex adsorbent [Cu(II)-IIP] from alginate and chitosan was prepared by a three-step process of beading–combining–crosslinking with Cu²⁺ as the template ion. The Cu(II)-IIP showed higher capacity and selectivity for Cu(II) than the non-imprinted polymer. The theoretical maximum adsorption capacity of Cu(II)-IIP reached 83.33 mg/g, and the separation factor (α) for Cu(II) versus Zn(II) was 2.28. The adsorption of Cu²⁺ onto the Cu(II)-IIP was perfectly described by the Langmuir isotherm model. The adsorption kinetics agreed with the pseudo-first-order model in the first 8 h and more fitted pseudo-second-order model after then. Weber–Morris model confirmed that the adsorption rate would be controlled dominantly by the intraparticle diffusion and the inner surface binding. Moreover, the Cu(II)-IIP complex adsorbent exhibited good regeneration, and the adsorption capacity was stable within the first three adsorption–desorption cycles without significant reduction.

Keywords Chitosan · Alginate · Complex · Ion imprinting · Cu(II) ion · Adsorption

Introduction

Heavy metal ions in the aqueous environment remains a major issue because of their high toxicity, persistence and susceptible carcinogenic effect [1–4]. Selective recognition of metal ions is a real challenge for a wide range of applications in the analytical field including extraction, detection and quantification. For that purpose, ion-imprinted polymers (IIPs) have been increasingly developed during the past decades [5, 6]. Similar to molecularly imprinted polymers (MIPs), IIPs are a class of well-tailored functional materials, in which specific cavities that match the target ion

✉ Xiao Li
lxzwy@fzu.edu.cn

¹ College of Chemical Engineering, Fuzhou University, Fuzhou 350108, China

(namely the template ion) in shape, size and functional groups are distributed, rendering high binding affinity and specificity to the target ion [7, 8]. The crosslinking of linear chain polymers carrying metal-binding groups is a well-developed technique used to prepare IIPs [9, 10]. This approach is simpler than polymerization and can avoid the use of an initiator. Moreover, the IIPs possess good chemical stability [11].

The development of metal ion imprinting technology is of significance for the environment, materials, life science and other fields. Nishide [12] prepared a metal ion-imprinted polymer for the first time in 1976 and opened a precedent for the study of metal ion imprinting. Su et al. [13, 14] prepared Ni(II) ion-imprinted polymers by using surface ion imprinting technique with mycelia and chitosan as raw materials and epichlorohydrin as crosslinking agent. The adsorption capacity for Ni²⁺ reached 82.5 mg/g in a suitable condition. An and Gao [15, 16] grafted polyethylenimine to the surface of silica gel particles and prepared metal ion [Cr(III), Cu(II)]-imprinted polymer IIP-PEI/SiO₂ with epichlorohydrin as crosslinking agent. The adsorption capacity of IIP-PEI/SiO₂ enhanced nearly two times compared to PEI/SiO₂, and the selectivity for the template ion was excellent. Araki et al. [17] applied a surface imprinting technique to prepare a Zn(II) ion-imprinted polymeric membrane, which showed higher adsorption affinity and permeation selectivity towards Zn²⁺ than the non-imprinted counterpart.

Natural polymer materials (cellulose, chitin and sodium alginate, etc.) have been widely used in the separation of heavy metals in the water environment. In recent years, natural polymer materials were tried to be combined with the ion imprinting technology to prepare the adsorbent materials with low cost, biodegradability and specific adsorption for metal ions. Cellulose is a natural polymer with rich sources, non-toxicity and wide application. Lin [18] grafted acrylic acid onto cellulose and prepared Pb(II) ion-imprinted polymer microspheres by inverse suspension polymerization. The imprinted microspheres showed a high adsorption amount (412 mg/g) and excellent selectivity for Pb²⁺.

In this paper, sodium alginate and chitosan, two kinds of natural polymer materials, are employed as matrix to explore a novel complex adsorbent for Cu(II) ions by using ion imprinting technology, where the electrostatic interaction between the carboxyl groups of sodium alginate and the protonated amino groups of chitosan is fully used to prepare the alginate–chitosan (ALG–CTS) complex adsorbent and improve the adsorption performance comparing with chemical modification. Furthermore, the adsorbent has a regular shape and good dispersibility which is better for recycling and reuse. This study is of great significance to the treatment of heavy metal pollution in water environment.

Experimental

Materials

Sodium alginate (SA) was obtained from Pharmaceutical Group Shanghai Chemical Reagent Company (China). Chitosan (CTS) and

2-[(5-bromo-2-pyridinyl)-azo]-5-diethylamino-phenol were purchased from Sinopharm Chemical Reagent Co., Ltd. (China). Anhydrous calcium chloride and acetic acid were obtained from Shanghai Reagent Plant (China). $\text{CuCl}_2 \cdot 2\text{H}_2\text{O}$ was purchased from Shantou Guanghua Chemical Factory (China). Glutaraldehyde was obtained from Tianjin Fuchen Chemical Reagent Factory (China). $\text{ZnSO}_4 \cdot 7\text{H}_2\text{O}$ was purchased from Guangdong Guanghua Chemical Factory Co., Ltd. (China). All other reagents were of analytical grade and were used without further purification. All solutions were prepared with deionized water.

Preparation of Cu(II)-IIP Complex Adsorbent

The spherical Cu(II)-IIP complex adsorbent based on SA and CTS was prepared by a three-step process of beading–combining–crosslinking.

Beading: 0.6 g SA was dissolved in 59.4 g of deionized water to obtain 1% of SA solution. Then, the SA solution was dropped by syringe into 60 mL of mixed solution (1.5% CaCl_2 and 0.5% CuCl_2) to form alginate (ALG) gel beads. The gel beads were washed with deionized water to remove Cl^- on the surface after static incubation for 1 h.

Combining: 0.4 g of CTS and 75 mg of Cu(II) were dissolved in 39.6 g of 1% acetic acid solution to obtain 1% of CTS solution. The washed ALG gel beads were then transferred to the CTS solution for 24 h of combination. The ALG–CTS complex gel beads were thus obtained and washed with deionized water to remove the unreacted CTS on the surface.

Crosslinking: the ALG–CTS complex gel beads were transferred to 4.17% (w/w) of glutaraldehyde solution to crosslink at 25 °C for 12 h. The residual glutaraldehyde on the crosslinked complex gel beads was washed away with deionized water at 60 °C.

Finally, the crosslinked complex gel beads were treated with 1 mol/L HCl to completely elute the template Cu(II) ions. After that, the samples were dried at 50 °C under vacuum for 12 h. The obtained product was the Cu(II) ion-imprinted ALG–CTS complex adsorbent and was labelled as Cu(II)-IIP.

For comparison, the non-ion-imprinted ALG–CTS complex adsorbent (NIP) was also prepared under the same conditions as above but without adding template Cu(II) ions.

Characterization

The morphology of the Cu(II)-IIP before drying was observed by ZSA302 zoom stereomicroscope (Chongqing Optical Instrument Co., Ltd., China). The Cu(II)-IIP was freeze-dried and observed by HIROX SH-4000M desktop scanning electron microscope (Questar China Limited, USA). The infrared spectra were recorded by Spectrum-2000 FTIR (Perkin-Elmer, USA) with a solid KBr tablet method. The adsorption capacity of the adsorbent was detected by Cary 50 UV spectrophotometer (Varian, USA) at room temperature.

Batch adsorption

A total of 0.01 g of adsorbent was mixed with 50 mL of Cu^{2+} solutions with different initial concentrations and pH values in a conical flask. The pH value was adjusted by 0.1 mol/L HCl or 0.1 mol/L NaOH. The batch experiments were carried out in a shaking air bath at 25 °C for 24 h. The adsorbent was separated by filtration, and the concentration of Cu^{2+} in solution was analysed using an UV spectrophotometer. The amount of Cu(II) bound on Cu(II)-IIP and NIP was calculated according to the following equation:

$$q_e = \frac{(C_0 - C_e)V}{m} \quad (1)$$

where q_e is the equilibrium adsorption capacity (mg/g); C_0 and C_e are the initial and equilibrium concentrations of Cu^{2+} in the adsorption solution ($\mu\text{g/mL}$), respectively; V is the volume of the adsorption solution (mL); and m is the mass of adsorbent (g).

Selectivity of Adsorption

The selective adsorption test of Cu(II)-IIP towards Cu^{2+} was implemented with Zn^{2+} as the competitor. A total of 0.01 g of Cu(II)-IIP was added into 50 mL of solution with 60 mg/L of Cu(II) or Zn(II) at pH 5.73. The residual concentration of ions in the solution was measured at intervals by a UV spectrophotometer until the adsorption reached equilibrium. Imprinting factor (β) and separation factor (α) were used to evaluate the selectivity of Cu(II)-IIP and were calculated as follows.

$$K_d = \frac{C_p}{C_s} \quad (2)$$

$$\beta = \frac{K_{d\text{IIP}}}{K_{d\text{NIP}}} \quad (3)$$

$$\alpha = \frac{K_{d\text{Cu}}}{K_{d\text{Zn}}} \quad (4)$$

where K_d is the static partition coefficient (mL/g); C_p is the equilibrium concentration of metal ions on the adsorbent ($\mu\text{g/g}$); C_s is the equilibrium concentration of metal ions in the solution ($\mu\text{g/mL}$); $K_{d\text{IIP}}$ and $K_{d\text{NIP}}$ are the static partition coefficients of Cu(II) for Cu(II)-IIP and NIP, respectively; and $K_{d\text{Cu}}$ and $K_{d\text{Zn}}$ are the static partition coefficients of Cu(II) and Zn(II), respectively. β reflects the difference of Cu(II)-IIP and NIP in template ion recognition. The greater β indicates the better

imprinting effect. α reflects the selectivity of adsorbent for template ion. If $\alpha > 1$, it indicates a certain selectivity, and the greater α means the better selectivity.

Regeneration

The regeneration of an adsorbent decides the economic success of the adsorption process. Desorption experiments of Cu(II)-adsorbed Cu(II)-IIP were performed at ambient temperature for 80 min using 1 mol/L hydrochloric acid solution as the stripping agent. After that, Cu(II)-IIP was separated and washed with distilled water and then dried in a vacuum oven at 50 °C. The adsorption–desorption cycle was repeated five times to assess the reusability of the Cu(II)-IIP complex adsorbent.

Results and Discussion

Imprinting Process of Cu(II)-IIP

In the preparation of Cu(II)-IIP complex adsorbent, two kinds of natural polymer materials, SA and CTS, were adopted as the functional matrix. The imprinting process is suggested schematically in Fig. 1. The carboxylate ions of SA possibly formed ionic complexes with Cu^{2+} while the hydroxyls of SA could form coordinate bonds to Cu^{2+} . Thanks to these two kinds of chemical bonds, many stable structures like eggbox were formed in SA. This was the first type of imprinting site of Cu(II)-IIP, and the whole structure was negatively charged. Meanwhile, coordination bonds could be easily formed between the aminos of chitosan and Cu^{2+} . This was the second type of imprinting site of Cu(II)-IIP, and the whole structure of acidified CTS was positively charged. An ionic complex could be established between

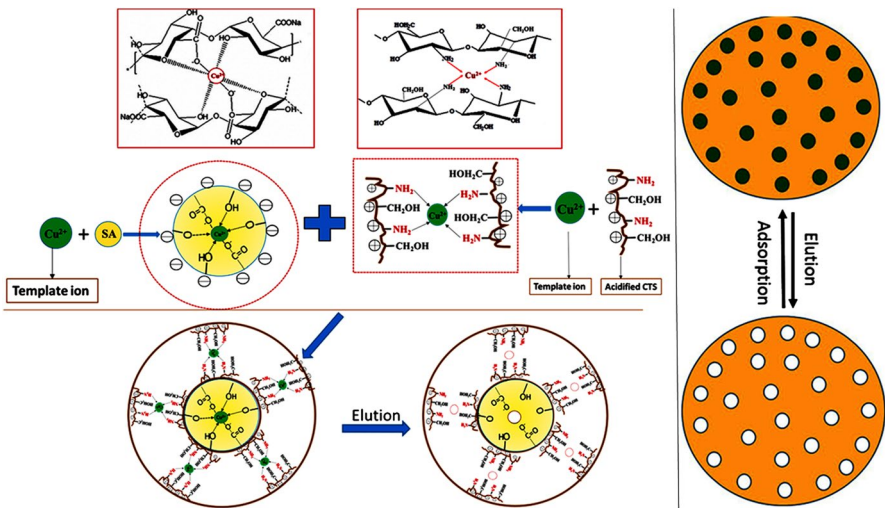


Fig. 1 Schematic preparation of Cu(II)-IIP complex adsorbent

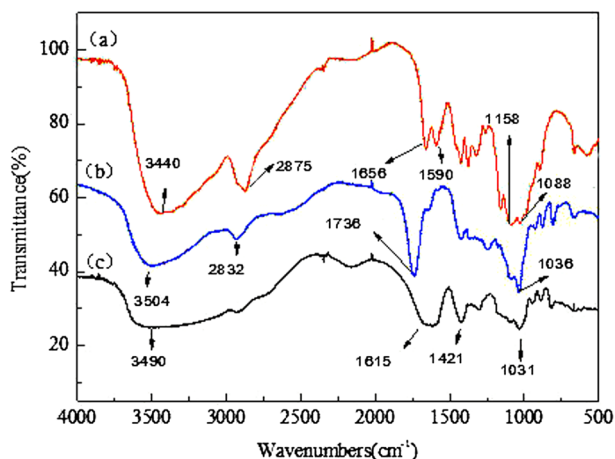


Fig. 2 FTIR spectra: **a** CTS, **b** Cu(II)-IIP and **c** SA

Table 1 Characteristic peaks of FTIR spectra

SA (cm ⁻¹)	CTS (cm ⁻¹)	Cu(II)-IIP (cm ⁻¹)
3490: ν (O–H)	3440: ν (O–H) [including ν (N–H)]	3504: ν (O–H) [including ν (N–H)]
	2875: ν (C–H)	2832: ν (C–H)
1615: ν_{as} (COO ⁻)	1656: ν (C=O) (amide I)	1736: ν (C=O)
1421: ν (COO ⁻)	1590: δ (N–H) [including 1550 amide II: ν (C–N) + δ (N–H)]	
1031: ν_{as} (C–O–C)	1158: ν_{as} (C–O–C) + ν (C–N)	1036: ν_{as} (C–O–C)
	1088: ν_{as} (skeleton)	

the eggbox-like structures and the acidified CTS via ionic interaction, although the strength of the eggbox-like structures was actually deficient due to the water dissociation [19]. Therefore, the ionic interaction of COO⁻ and NH₃⁺ played an important role in the preparation of Cu(II)-IIP. After the template Cu²⁺ was removed by elution, the Cu(II)-IIP could rebind Cu²⁺ selectively. The imprinting sites with the proper size and oriented groups exactly for Cu²⁺ in Cu(II)-IIP would contribute to a high adsorption efficiency and selectivity for Cu²⁺ due to metal–ligand chemistry [20].

FTIR Spectra

The spectra of SA, CTS and Cu(II)-IIP are shown in Fig. 2, and the typical peaks of the chemical bonds in the three samples are presented in Table 1 [21].

As shown in Fig. 2 and Table 1, the typical peaks at 1656 and 1590 cm^{-1} attributing to the amide in CTS disappeared after imprinting. Similarly, the peaks at 1615 and 1421 cm^{-1} attributing to the antisymmetric and symmetric stretching vibration of $-\text{COO}^-$ in SA also disappeared after imprinting. However, a new peak at 1736 cm^{-1} was observed in the Cu(II)-IIP. The results of FTIR revealed that a reaction occurred between the $-\text{NH}_2$ in CTS and $-\text{COO}^-$ in SA during the imprinting process.

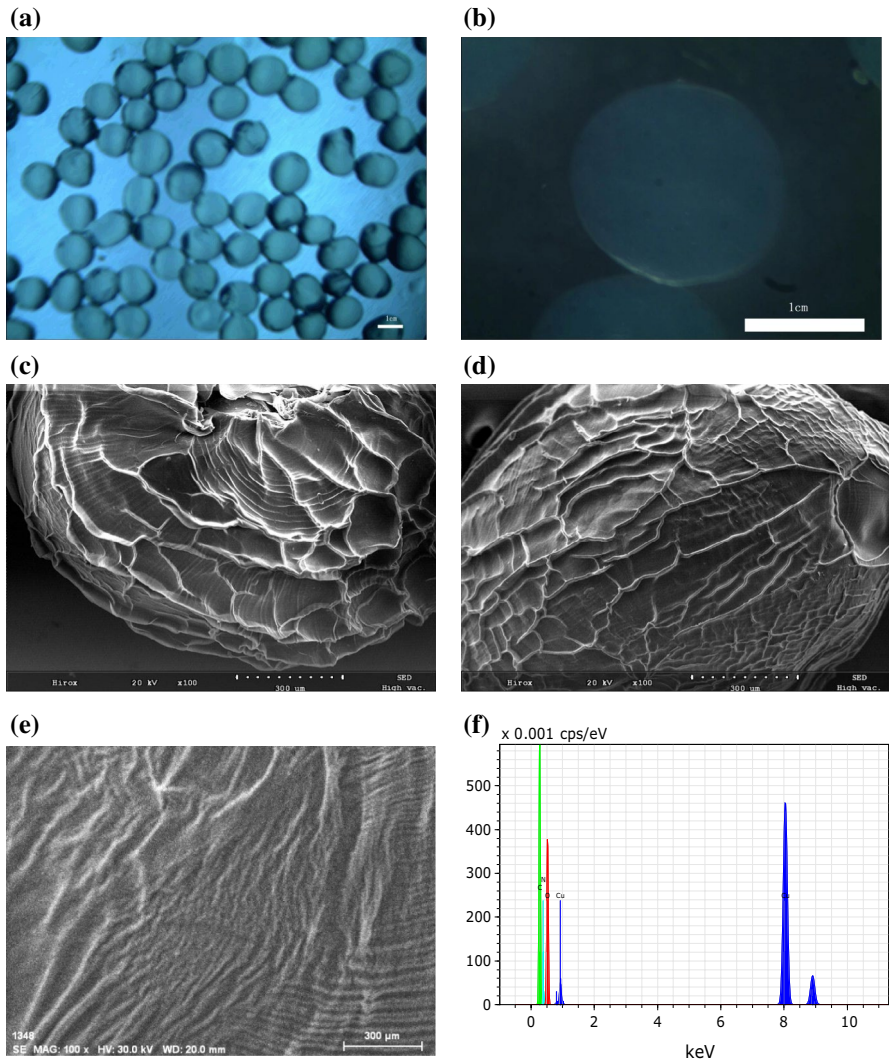


Fig. 3 Surface structures of Cu(II)-IIP and NIP. **a** Stereomicroscopic light image of wet Cu(II)-IIP beads, **b** stereomicroscopic backlight image of wet Cu(II)-IIP beads, **c** SEM of freeze-dried NIP beads ($\times 100$), **d** SEM of freeze-dried Cu(II)-IIP beads ($\times 100$), **e** SEM of freeze-dried Cu(II)-IIP beads after adsorption of Cu^{2+} ($\times 100$) and **f** energy spectrum of freeze-dried Cu(II)-IIP beads after adsorption of Cu^{2+}

SEM Analysis

Figure 3a, b is the stereomicroscopic images of the wet Cu(II)-IIP beads under light and backlight conditions, respectively. As shown in the pictures, the Cu(II)-IIP beads were in the state of hydrogel with a certain content of moisture and smooth surface. The particle size was uniform and the average size was about 1.78 mm.

The SEM of freeze-dried NIP and Cu(II)-IIP beads is shown in Fig. 3c, d. A lot of folds were observed on the surfaces of the two kinds of beads due to the dehydration of the gel beads. However, the degree of surface folds on Cu(II)-IIP was smaller than that on NIP. It was attributed to the structure change in the presence of Cu^{2+} during imprinting, which resulted in a slower rate of water loss.

The SEM of Cu(II)-IIP complex beads after adsorption of Cu^{2+} is shown in Fig. 3e. The more surface folds were observed and they arranged closely, indicating that the presence of Cu^{2+} had influence on the surface morphology of Cu(II)-IIP complex adsorbent, also confirming that Cu^{2+} could change the three-dimensional network structure of the complex gel beads and then affected the water loss process. Figure 3f is the corresponding electron diffraction energy spectrum diagram of Fig. 3e. A strong peak of element Cu showed that the Cu(II)-IIP has a strong adsorption ability for Cu(II). At the same time, the peak of element N was also observed, which meant that CTS was successfully combined with ALG to form composite. And the composite was stable enough to endure elution to produce Cu(II)-IIP.

Adsorption Experiments

Influence of pH Value

The pH value of solution is one of the most important parameters governing the uptake of metal ions on adsorbents [22]. The effect of pH value on Cu^{2+} adsorption by

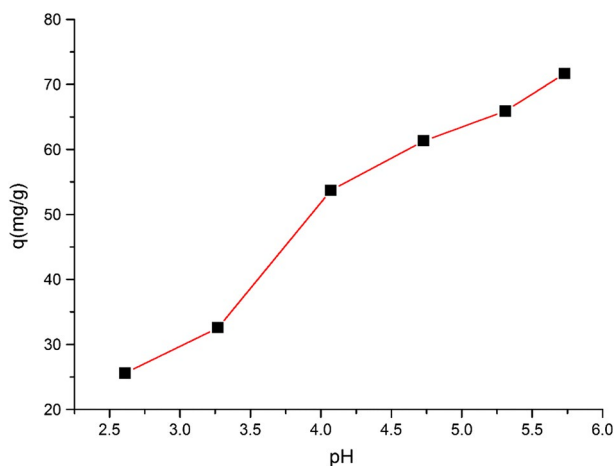


Fig. 4 Effect of pH value on Cu^{2+} adsorption capacity

Cu(II)-IIP was investigated at different pH values ranging from 2.61 to 5.73, and the results are shown in Fig. 4.

As shown in Fig. 4, the adsorption of Cu^{2+} on Cu(II)-IIP was pH-dependent, and the adsorption capacity increased as the solution pH value increased from 2.61 to 5.73. When the pH value was below 4.07, the adsorption capacities of Cu(II)-IIP was very low, which was mainly due to the protonation of the $-\text{NH}_2$ group moieties and their diminishing ability to chelate Cu^{2+} [23]. The adsorption of Cu^{2+} on Cu(II)-IIP was higher when the pH value was over 4.73. The possible reason was that the NH_3^+ groups were deprotonated and their chelating ability was recovered. When the pH value of solution was increased to 6.0, Cu(II) was deposited as $\text{Cu}(\text{OH})_2$. Thus, the pH value of solution should be adjusted to pH 5.73 to obtain the optimal adsorption efficiency.

Adsorption Isotherm

Figure 5 shows the adsorption isotherm of Cu(II)-IIP towards Cu^{2+} at pH 5.73. It could be observed that the equilibrium adsorption capacity (q_e) increased sharply in the low initial concentration of Cu^{2+} and then increased slowly until saturation.

In order to describe the Cu(II) distribution between the liquid and adsorbent phases and the maximum adsorption capacity of Cu(II)-IIP, Langmuir and Freundlich isotherm models were used to fit the adsorption process as follows.

$$\frac{C_e}{q_e} = \frac{1}{bq_{\max}} + \frac{C_e}{q_{\max}} \tag{5}$$

$$\ln q_e = \ln k_f + \frac{1}{n} \ln C_e \tag{6}$$

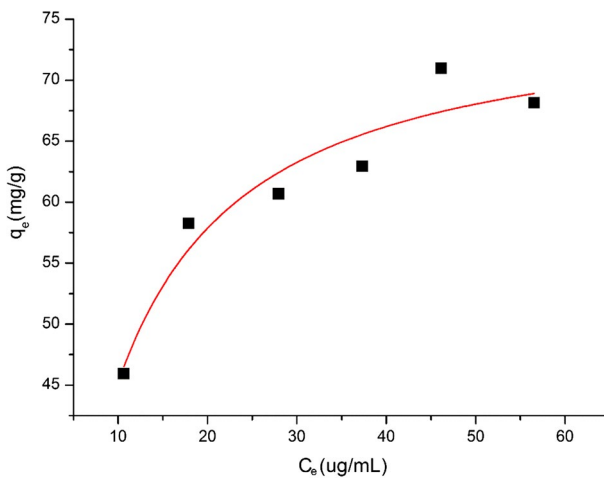


Fig. 5 Adsorption isotherm of Cu^{2+} on Cu(II)-IIP

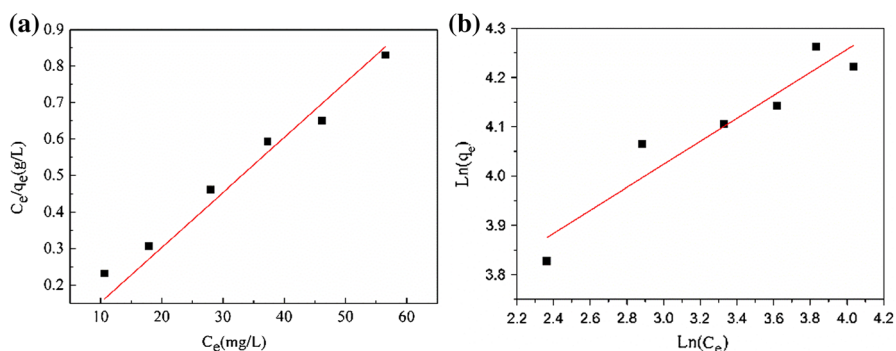


Fig. 6 Fitting results of adsorption isotherm of Cu^{2+} on Cu(II)-IIP. **a** Langmuir model and **b** Freundlich model

Table 2 Langmuir and Freundlich isotherm parameters for Cu(II)-IIP

Adsorbent	Langmuir model			Freundlich model		
	q_{\max} (mg/g)	b	R^2	k_f	n	R^2
Cu(II)-IIP	83.33	0.1395	0.993	27.77	4.288	0.878

where q_e is the equilibrium adsorption capacity (mg/g); C_e is the equilibrium concentration of Cu^{2+} ($\mu\text{g}/\text{mL}$); q_{\max} is the maximum adsorption capacity (mg/g); b is the Langmuir constant that represents the affinity between solute and adsorbent; and k_f and n are Freundlich constants related to the adsorption capacity and the adsorption intensity, respectively.

The fitting results of Langmuir and Freundlich isotherms for the adsorption of Cu^{2+} on Cu(II)-IIP are shown in Fig. 6 and Table 2. According to the value of correlation coefficient (R^2), the Langmuir model ($R^2 = 0.993$) was more suitable than the Freundlich model ($R^2 = 0.878$) for describing the adsorption process. The maximum adsorption capacity obtained from Langmuir model was 83.33 mg/g, which indicated that the Cu(II)-IIP had a strong affinity for Cu^{2+} .

Adsorption Kinetics

Figure 7 shows the time dependence of the adsorption amounts of Cu^{2+} on Cu(II)-IIP with 60 $\mu\text{g}/\text{ml}$ of the initial Cu^{2+} concentration and contact time from 0 to 25 h at pH 5.73. It could be seen from Fig. 7 that the adsorption amounts increased rapidly during the first 12 h and then leveled off as equilibrium was reached. The high adsorption rate at the beginning was attributed to the sufficient adsorption sites on Cu(II)-IIP with strong chelation and good affinity towards Cu^{2+} [23].

Adsorption kinetics is usually used to confirm the rate controlling step of adsorption. To reveal the mechanism of adsorption, the adsorption kinetics for Cu^{2+} onto the Cu(II)-IIP were investigated by three kinetics models, namely Lagergren pseudo-first-order model, pseudo-second-order model and Weber–Morris model. The linear forms of the three models are expressed as follows:

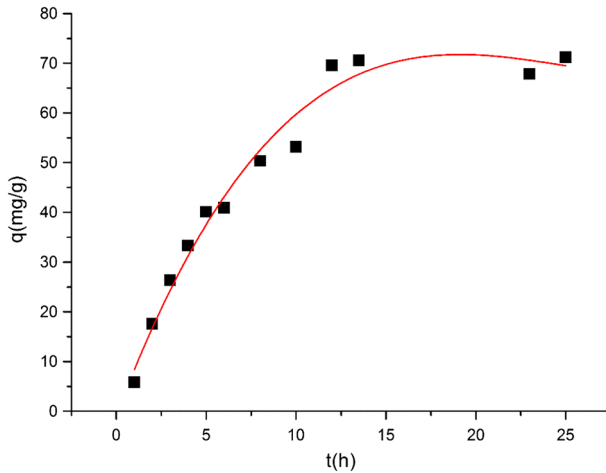


Fig. 7 Variation of adsorption amount of Cu²⁺ with contact time

$$\ln(q_e - q_t) = \ln q_e - k_1 t \tag{7}$$

$$\frac{t}{q_t} = \left(\frac{1}{k_2 q_e^2} \right) + \frac{t}{q_e} \tag{8}$$

$$q_t = k_{\text{dif}} t^{0.5} \tag{9}$$

where q_e and q_t are the adsorption capacity (mg/g) at equilibrium and at time t (h), respectively; k_1, k_2, k_{dif} are the adsorption rate constants. The adsorption kinetic constants and correlation coefficients are summarized in Table 3.

According to the data presented in Fig. 8 and Table 3, the kinetic curve fitted the pseudo-first-order model in the first 8 h, and the pseudo-second-order mechanism was predominant after 8 h. This meant that the Cu²⁺ diffusion onto and in the Cu(II)-IIP could be the rate controlling step at first. Then, the adsorption was dominated by the intraparticle diffusion and the inner surface binding. The inner surface binding was associated with the chemisorption of Cu²⁺ onto the two types of imprinting sites in the Cu(II)-IIP as illustrated in Fig. 1.

Weber–Morris model was usually used to estimate whether the intraparticle diffusion was the rate controlling step of adsorption. According to the Weber–Morris model,

Table 3 Fitting results of adsorption kinetics models

Adsorbent	Pseudo-first-order			Pseudo-second-order			Weber–Morris model	
	k_1 (1/h)	$q_{e,m}$ (mg/g)	R^2	k_2 (g/mg h)	$q_{e,m}$ (mg/g)	R^2	k_{dif} (mg/g h ^{1/2})	R^2
Cu(II)-IIP	0.159	73.6	0.984	0.003	82.5	0.949	23.52	0.981

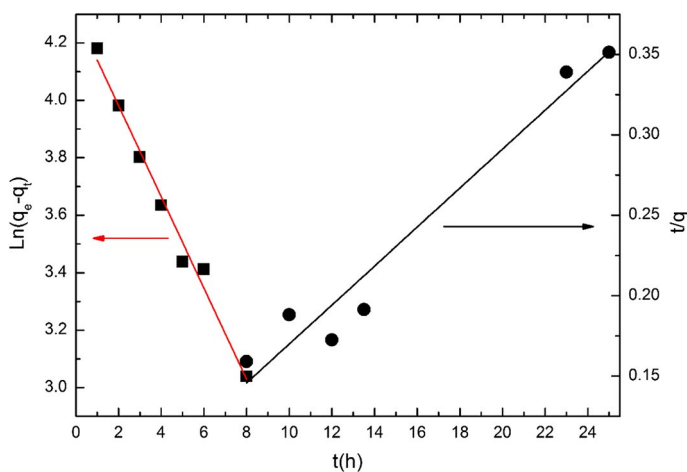


Fig. 8 Pseudo-first-order model (filled square) for Cu^{2+} adsorption before 8 h and pseudo-second-order model (filled circle) for Cu^{2+} adsorption after 8 h

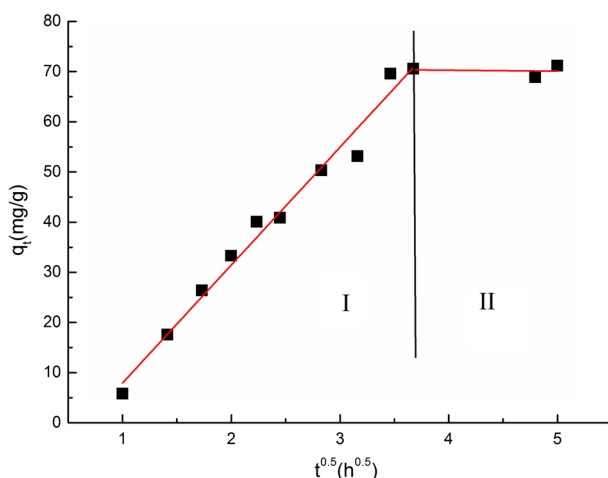


Fig. 9 Fitting plot of intraparticle diffusion model for Cu^{2+} adsorption

the fitting plot of q_t versus time $t^{0.5}$ is shown in Fig. 9 and the regression parameters are listed in Table 3. It showed that the Cu^{2+} adsorption onto the Cu(II)-IIP was not always linear and could be divided into two stages, which demonstrated that there are not only one rate limiting step during the Cu^{2+} adsorption.

From the above discussion, an explanation about the kinetic process of adsorption of Cu^{2+} onto Cu(II)-IIP was suggested. At the beginning, the adsorption was fast owing to the diffusion of Cu^{2+} from the solution to the external surface of Cu(II)-IIP. Then, the Cu^{2+} gradually passed through the apertures in Cu(II)-IIP at a lower speed, and they were subsequently bound to the imprinting sites through the

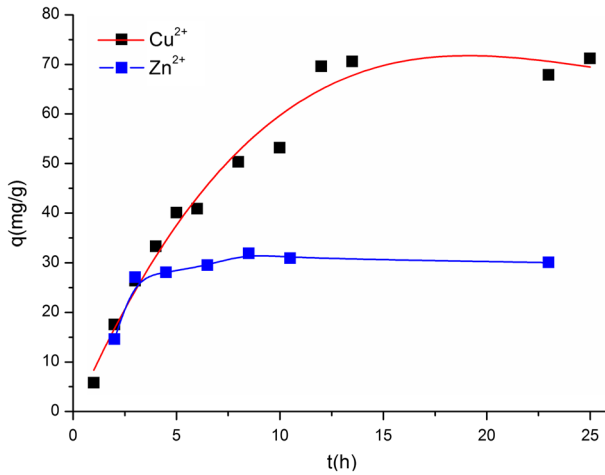


Fig. 10 Variation of adsorption amount of metal ions with contact time

Table 4 Selective adsorption of Cu(II)-IIP for Cu²⁺ versus Zn²⁺

Metal ion	Cu(II)-IIP			NIP			β
	q (mg/g)	K_d (mL/g)	α	q (mg/g)	K_d (mL/g)	α	
Cu ²⁺	71.15	31.09	2.28	50.92	20.44	1.72	1.52
Zn ²⁺	36.03	13.65	–	31.82	11.87	–	–

electrostatic attraction and metal–ligand interaction. The intraparticle diffusion and the inner surface binding were the main rate controlling steps. Finally, the adsorption equilibrium occurred when the imprinting sites were all occupied and the intraparticle diffusion reached steady state.

Selectivity of Cu(II)-IIP

Zn(II) ion was chosen as the competitor ion due to the fact that Zn²⁺ has the same charge and similar size to Cu²⁺. As shown in Fig. 10, the adsorption amount of Cu(II)-IIP did not stop increasing with contact time until 12 h for Cu(II) but 5 h for Zn(II) when the equilibrium reached. The equilibrium adsorption capacity of Cu²⁺ was clearly higher than that of Zn²⁺. It implied that Cu(II)-IIP exhibited a much stronger affinity to Cu²⁺ than that to Zn²⁺.

Static distribution coefficients, separation factor (α) and imprinting factor (β) are calculated and summarized in Table 4. From Table 4, the separation factor of Cu(II)-IIP for Cu(II) versus Zn(II) reached 2.28 and the imprinting factor reached 1.52 compared with NIP. It confirmed that the Cu(II)-IIP had a certain selective recognition for Cu(II). As in Fig. 1, the imprinted sites with specific recognition groups in a predetermined orientation for Cu²⁺ were formed in the Cu(II)-IIP. Cu²⁺ could be rebound to the imprinting sites while Zn²⁺ could not match the imprinting sites well

Fig. 11 Effect of the time of reuse on adsorption capacity

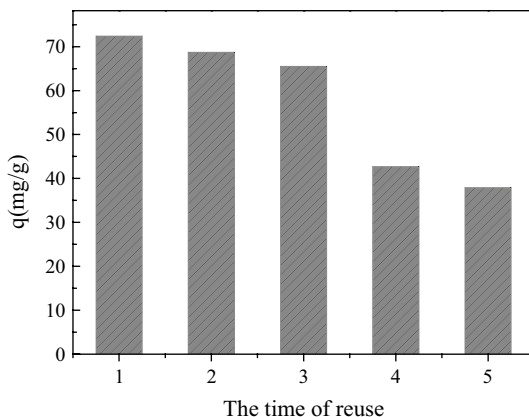


Table 5 The adsorption for Cu(II) of some absorbents reported in the literature

Adsorbents	q_{\max} (mg/g)	Equilibrium time (h)	Optimum pH	References
Cu(II)-MICA	46.25	6.0	5.5	[24]
Cu(II)-MIIP	24.20	0.17	5.0	[25]
Cu(II)-IIP	76.00	0.17	5.0	[26]
Cu(II)-MICA	71.36	4.0	5.5	[27]
CTS-ECH-TPP	166.94	20.0	6.0	[28]
Cu-ALG-CTS	70.54	13.0	–	[29]
Cu(II)-IIP	83.33	8.0	5.7	This work

in shape, size, and functional groups. Therefore, the Cu(II)-IIP showed the specific selectivity and higher adsorption capacity for Cu^{2+} .

Regeneration and Reuse of Cu(II)-IIP

The stability and reusability of Cu(II)-IIP were investigated by means of adsorption–desorption cycle, and the results are illustrated in Fig. 11. It was found that the adsorption capacity of Cu(II)-IIP for Cu^{2+} was stable in the first three cycles without significant reduction. This referred that the Cu(II)-IIP could be regenerated effectively and reused to lower the cost.

Adsorption Performance

Our work and some other reported absorbents for adsorption of Cu(II) are listed in Table 5. The prepared Cu(II)-IIP has high binding capacity for Cu(II) and possesses potential application in the removal of Cu(II) from wastewater.

Conclusions

A novel Cu(II) ion-imprinted complex adsorbent (Cu(II)-IIP) from alginate and chitosan was successfully prepared by a three-step process of beading–combining–crosslinking. FTIR suggested that the ionic interaction occurred between the amino of chitosan and the carboxyl of alginate during imprinting. SEM indicated that the morphology of the Cu(II)-IIP was affected by the imprinting process. The adsorption and selectivity of Cu(II)-IIP for Cu^{2+} were investigated in detail. It was found that the adsorption amount of Cu^{2+} varied obviously with pH value, initial Cu^{2+} concentration and contact time. The suitable pH value for favourable Cu^{2+} adsorption was 5.73. The adsorption isotherm well fitted Langmuir model, which indicated that the monolayer coverage of Cu^{2+} was formed at the surface of Cu(II)-IIP and the theoretical maximum adsorption capacity was 88.33 mg/g. The adsorption of Cu(II)-IIP for Cu^{2+} performed rapidly at first and then slowed down until reaching equilibrium. Pseudo-first-order model, pseudo-second-order model and Weber–Morris model were used to fit the adsorption behaviour, which suggested that the adsorption rate would be controlled dominantly by the intraparticle diffusion and the inner surface binding. Competitive adsorption test showed that the Cu(II)-IIP had the specific selectivity and higher adsorption capacity for Cu^{2+} versus Zn^{2+} with a separation factor of 2.28 due to the Cu^{2+} imprinting sites. The regeneration experiments demonstrated that the Cu(II)-IIP could be repeatedly used without significant loss in adsorption capacity. These conclusions suggested that the Cu(II)-IIP could be used as a feasible adsorbent for selective removal of Cu(II) from water.

Acknowledgements This work was financially supported by the Science and Technology Guiding Projects of Fujian Province (No. 2015H0019) and the Natural Science Foundation of Fujian Province of China (No. 2015J01197).

References

1. Chipasa KB (2003) Accumulation and fate of selected heavy metals in a biological wastewater treatment system. *Waste Manage* 23:135–143
2. Memon S, Tabakci M, Roundhill DM, Yilmaz M (2005) A useful approach toward the synthesis and metal extractions with polymer appended thioalkyl calix[4]arenes. *Polymer* 46:1553–1560
3. Utgikar VP, Chaudhary N, Koeniger A, Tabak HH, Haines JR, Govind R (2004) Toxicity of metals and metal mixtures: analysis of concentration and time dependence for zinc and copper. *Water Res* 38:3651–3658
4. Hasegawa H, Rahman IMM, Nakano M, Begum ZA, Egawa Y, Maki T (2011) Recovery of toxic metal ions from washing effluent containing excess aminopolycarboxylate chelant in solution. *Water Res* 45:4844–4854
5. Branger C, Meouche W, Margailan A (2013) Recent advances on ion-imprinted polymers. *React Funct Polym* 73:859–875
6. Lopes Pinheiro SC, Descalzo AB, Raimundo IM Jr, Orellana G, Moreno-Bondi MC (2012) Fluorescent ion-imprinted polymers for selective Cu(II) optosensing. *Anal Bioanal Chem* 402:3253–3260
7. Tarley CRT, Andrade FN, de Santana H, Zaia DAM, Beijo LA, Segatelli MG (2012) Ion-imprinted polyvinylimidazole-silica hybrid copolymer for selective extraction of Pb(II): characterization and metal adsorption kinetic and thermodynamic studies. *React Funct Polym* 72:83–91

8. Wang J, Ding L, Wei J, Liu F (2014) Adsorption of copper ions by ion-imprinted simultaneous interpenetrating network hydrogel: thermodynamics, morphology and mechanism. *Appl Surf Sci* 305:412–418
9. Shawky HA (2009) Synthesis of ion-imprinting chitosan/PVA crosslinked membrane for selective removal of Ag(I). *J Appl Polym Sci* 114:2608–2615
10. Wang X, Zhang L, Ma C, Song R, Hou H, Li D (2009) Enrichment and separation of silver from waste solutions by metal ion imprinted membrane. *Hydrometallurgy* 100:82–86
11. Lin CX, Liu MH, Zhan HY (2011) Pb(II)-imprinted polymer prepared by graft copolymerization of acrylic acid onto cellulose. *Adv Mater Res* 295–297:2045–2048
12. Nishide H, Tsuchida H (1976) Selective adsorption of metal ions on poly (4-vinylpyridine) resins in which the ligand chain is immobilized by crosslinking. *Macromol Chem Phys* 177:2295–2310
13. Su H, Zhao Y, Li J, Tan TW (2006) Biosorption of Ni²⁺ by the surface molecular imprinting adsorbent. *Process Biochem* 41:1422–1426
14. Su H, Chen S, Tan T (2007) Surface active site model for Ni²⁺, adsorption of the surface imprinted adsorbent. *Process Biochem* 42:612–619
15. An F, Gao B (2009) Adsorption characteristics of Cr(III) ionic imprinting polyamine on silica gel surface. *Desalination* 249:1390–1396
16. Gao B, An F, Zhu Y (2007) Novel surface ionic imprinting materials prepared via couple grafting of polymer and ionic imprinting on surfaces of silica gel particles. *Polymer* 48:2288–2297
17. Araki K, Maruyama T, Kamiya N, Goto M (2005) Metal ion-selective membrane prepared by surface molecular imprinting. *J Chromatogr B* 818:141–145
18. Lin CX, Zhan HY, Liu MH, Zhang JJ, Fu SY (2009) Homogeneous graft copolymerization of cellulose using an ionic liquid as a reaction medium. *China Pulp Pap* 28:32–35
19. Cai X, Li J, Zhang Z, Yang F, Dong R, Chen L (2014) Novel Pb²⁺ ion imprinted polymers based on ionic interaction via synergy of dual functional monomers for selective solid-phase extraction of Pb²⁺ in water samples. *ACS Appl Mater Interfaces* 6:305–313
20. Becker JJ, Gagné MR (2004) Exploiting the synergy between coordination chemistry and molecular imprinting in the quest for new catalysts. *Acc Chem Res* 37:798–804
21. Dong Y, Wang M, Wu Y, Ruan Y (2001) FTIR spectroscopic determinations of chitosan derivatives. *J Cellul Sci Technol* 9:42–56
22. Taty-Costodes VC, Fauduet H, Porte C (2005) Removal of lead (II) ions from synthetic and real effluents using immobilized *Pinus sylvestris* sawdust: adsorption on a fixed-bed column. *J Hazard Mater* 123:135–144
23. Luo X, Liu L, Deng F (2013) Novel ion-imprinted polymer using crown ether as a functional monomer for selective removal of Pb(II) ions in real environmental water samples. *J Mater Chem A* 1:8280–8286
24. Ren Y, Wei X, Zhang M (2008) Adsorption character for removal Cu(II) by magnetic Cu(II) ion imprinted composite adsorbent. *J Hazard Mater* 158:14–22
25. Luo X, Luo S, Zhan Y, Shu H, Huang Y, Tu X (2011) Novel Cu(II) magnetic ion imprinted materials prepared by surface imprinted technique combined with a sol-gel process. *J Hazard Mater* 192:949–955
26. Wang S, Zhang R (2006) Selective solid-phase extraction of trace copper ions in aqueous solution with a Cu(II)-imprinted interpenetrating polymer network gel prepared by ionic imprinted polymer (IIP) technique. *Microchim Acta* 154:73–80
27. Ren Y, Zhang M, Zhao D (2008) Synthesis and properties of magnetic Cu(II) ion imprinted composite adsorbent for selective removal of copper. *Desalination* 228:135–149
28. Laus R, Costa TG, Szpoganicz B, Favere VT (2010) Adsorption and desorption of Cu(II), Cd(II) and Pb(II) ions using chitosan crosslinked with epichlorohydrin-triphosphate as the adsorbent. *J Hazard Mater* 183:233–241
29. Zhang WY, Chen D, Li X, Ying XG (2012) Preparation and adsorption performance of Cu(II)-imprinted ALG-CTS complex microspheres. *Appl Mech Mater* 268–270:229–232